Biochimica et Biophysica Acta 1837 (2014) 1454–1462

Contents lists available at ScienceDirect

Biochimica et Biophysica Acta

journal homepage: www.elsevier.com/locate/bbabio

# Proteomic characterization and three-dimensional electron microscopy study of PSII–LHCII supercomplexes from higher plants ☆

Cristina Pagliano [a,*], Jon Nield [b], Francesco Marsano [c], Tillmann Pape [d], Simone Barera [c], Guido Saracco [a], James Barber [a,d,**]

[a] Applied Science and Technology Department, BioSolar Lab, Politecnico di Torino, Viale T. Michel 5, 15121 Alessandria, Italy
[b] School of Biological and Chemical Sciences, Queen Mary University of London, London E1 4NS, UK
[c] Department of Science and Technological Innovation, University of Piemonte Orientale, Viale T. Michel 11, 15121 Alessandria, Italy
[d] Department of Life Sciences, Faculty of Natural Sciences, Imperial College London, London SW7 2AZ, UK

ARTICLE INFO

*Article history:*
Received 23 September 2013
Received in revised form 24 October 2013
Accepted 5 November 2013
Available online 16 November 2013

*Keywords:*
Thylakoids
PSII–LHCII supercomplex
Proteomics
Transmission electron microscopy
Single particle analysis
Structure

ABSTRACT

In higher plants a variable number of peripheral LHCII trimers can strongly (S), moderately (M) or loosely (L) associate with the dimeric PSII core ($C_2$) complex via monomeric Lhcb proteins to form PSII–LHCII supercomplexes with different structural organizations. By solubilizing isolated stacked pea thylakoid membranes either with the α or β isomeric forms of the detergent n-dodecyl-D-maltoside, followed by sucrose density ultracentrifugation, we previously showed that PSII–LHCII supercomplexes of types $C_2S_2M_2$ and $C_2S_2$, respectively, can be isolated [S. Barera et al., Phil. Trans. R Soc. B 67 (2012) 3389–3399]. Here we analysed their protein composition by applying extensive bottom-up and top-down mass spectrometry on the two forms of the isolated supercomplexes. In this way, we revealed the presence of the antenna proteins Lhcb3 and Lhcb6 and of the extrinsic polypeptides PsbP, PsbQ and PsbR exclusively in the $C_2S_2M_2$ supercomplex. Other proteins of the PSII core complex, common to the $C_2S_2M_2$ and $C_2S_2$ supercomplexes, including the low molecular mass subunits, were also detected and characterized. To complement the proteomic study with structural information, we performed negative stain transmission electron microscopy and single particle analysis on the PSII–LHCII supercomplexes isolated from pea thylakoid membranes solubilized with n-dodecyl-α-D-maltoside. We observed the $C_2S_2M_2$ supercomplex in its intact form as the largest PSII complex in our preparations. Its dataset was further analysed *in silico*, together with that of the second largest identified sub-population, corresponding to its $C_2S_2$ subcomplex. In this way, we calculated 3D electron density maps for the $C_2S_2M_2$ and $C_2S_2$ supercomplexes, approaching respectively 30 and 28 Å resolution, extended by molecular modelling towards the atomic level. This article is part of a Special Issue entitled: Photosynthesis Research for Sustainability: Keys to Produce Clean Energy.



## 1. Introduction

Photosystem II (PSII) is one of the key protein complexes of the light reactions of photosynthesis, carrying out the conversion of solar energy into electrochemical potential energy required to drive the water splitting reaction which it catalyses, together with the production of reducing equivalents needed for driving $CO_2$ fixation. In plants and green algae, the PSII core complex has associated with it membrane-bound light-harvesting antenna complexes (LHCII), to form large macromolecular complexes called PSII–LHCII supercomplexes. The LHCII complexes, functioning as peripheral solar energy collectors, absorb most of the sunlight subsequently directed to the photochemical reaction centre (RC) of PSII.

In plants and green algae the PSII core complex is mainly embedded in the stacked regions of the thylakoid membranes where it is organized as a dimer, each monomer consisting of several proteins including: 1) D1 and D2, making up the photochemical RC; 2) CP47 and CP43, acting as inner antenna proteins; 3) several low molecular mass subunits (LMM subunits, <10 kDa), accounting for more than half of the entire

*Abbreviations:* BN-PAGE, blue native polyacrylamide gel electrophoresis; Chl, chlorophyll; 1D/2D SDS-PAGE, mono-dimensional/bi-dimensional sodium dodecyl sulphate polyacrylamide gel electrophoresis; 3D, three-dimensional; α-DM, n-dodecyl-α-D-maltoside; β-DM, n-dodecyl-β-D-maltoside; FEG, field emission gun; FSC, Fourier shell correlation; LC-ESI-MS/MS, liquid chromatography electrospray ionization tandem mass spectrometry; LHC, light harvesting complex; LMM, low molecular mass; MALDI-TOF/TOF, matrix-assisted laser desorption/ionization-time of flight/time of flight; MS, mass spectrometry; OEC, oxygen evolving complex; PS, photosystem; PTM, post translational modification; RC, reaction centre; TEM, transmission electron microscopy

☆ This article is part of a Special Issue entitled: Photosynthesis Research for Sustainability: Keys to Produce Clean Energy.

* Corresponding author. Tel.: +39 131 229301; fax: +39 131 229344.
** Correspondence to: J. Barber, Imperial College London, Department of Life Sciences, Faculty of Natural Sciences, London SW7 2AZ, UK. Tel.: +44 208 747 1165; fax: +44 207 594 5267.
*E-mail addresses:* cristina.pagliano@polito.it (C. Pagliano), j.nield@qmul.ac.uk (J. Nield), francesco.marsano@mfn.unipmn.it (F. Marsano), t.pape@imperial.ac.uk (T. Pape), simone.barera@mfn.unipmn.it (S. Barera), guido.saracco@polito.it (G. Saracco), j.barber@imperial.ac.uk (J. Barber).

0005-2728/$ – see front matter © 2013 Published by Elsevier B.V.
http://dx.doi.org/10.1016/j.bbabio.2013.11.004

complex and playing a role in stabilizing the binding of cofactors to the PSII core; and 4) the extrinsic polypeptides PsbO, PsbP, PsbQ and PsbR, forming the oxygen evolving complex (OEC) on the lumenal side of the membrane (for a recent review see [1]). Up to now the highest resolution structure available for the plant PSII core complex has been obtained by electron crystallography [2,3], which led to the assignment of the major subunits and location of their transmembrane helices. Moreover, crystal structures have been determined for the isolated extrinsic polypeptides PsbP [4] and PsbQ [5,6].

The most abundant PSII-associated LHCII complex, called "major", consists of homo- or hetero-trimers of Lhcb1, Lhcb2 and Lhcb3 polypeptides, usually occurring in a ratio of about 8:3:1 [7–9], whose high-resolution structures have been solved by X-ray crystallography [10,11]. According to these studies, all LHCIIs have three membrane-spanning regions connected by both stromal and lumenally-exposed loops and bind a total of 14 chlorophyll (Chl) molecules (8 Chl *a* and 6 Chl *b*) plus 4 carotenoid molecules. In addition, there are three "minor" LHCII antenna polypeptides, termed Lhcb4 (CP29), Lhcb5 (CP26) and Lhcb6 (CP24), which usually occur in monomeric form. So far, among the minor LHCII antenna proteins, the three-dimensional (3D) structure is available at high resolution only for Lhcb4 [12], revealing three transmembrane α-helices with 13 Chls binding sites (8 assigned as Chl *a* sites, 4 as Chl *b* sites and 1 putative mixed site occupied by both Chl *a* and Chl *b*) and 3 carotenoid binding sites.

A variable number of LHCII can associate with the dimeric PSII core complex to form different types of PSII–LHCII supercomplexes, named according to their composition [13]. The dimeric PSII core complex ($C_2$) strongly binds two copies of the monomeric Lhcb4 and Lhcb5 and two LHCII trimers (S-trimer) in order to form the $C_2S_2$ supercomplex [14], which can be regarded as a basic building block of PSII *in vivo*. Larger PSII–LHCII supercomplexes, containing two extra copies of the monomeric Lhcb6 with two additional LHCII trimers (M-trimer) moderately bound to the dimeric PSII core complex via Lhcb4 and Lhcb6, are known as $C_2S_2M_2$ and have been found to represent the basic organization of the PSII in *Arabidopsis thaliana* thylakoid membranes [13,15]. Occasionally even larger supercomplexes have been observed in isolated spinach thylakoids fragments, with one or two additional LHCII trimers (L-trimer) even more loosely bound to the dimeric PSII core complex via Lhcb6, and are known as $C_2S_2M_2L_{1-2}$ [16].

Note that the classification of LHCII trimers within the PSII–LHCII supercomplexes in strongly (S), moderately (M) or loosely (L) bound to the PSII dimeric core complex is based on susceptibility to solubilization by detergent. Thus the typology and composition of the isolated supercomplexes reflect the mildness of the detergent(s) used and the overall conditions of solubilization. By solubilizing isolated stacked pea thylakoid membranes either with the α or β isomeric forms of the detergent n-dodecyl-D-maltoside (DM), followed by sucrose density ultracentrifugation, we isolated PSII–LHCII supercomplexes with different molecular masses, shown to be respectively of types $C_2S_2M_2$ and $C_2S_2$, demonstrating the milder detergent action of α-DM with respect to β-DM [17].

In order to gain insights into the primary and tertiary structure of the isolated $C_2S_2M_2$ and $C_2S_2$ PSII–LHCII supercomplexes, we applied extensive multiple approaches of mass spectrometry (MS), combining bottom-up and top-down methods. Bottom-up MS techniques involve approaches where the intact protein is enzymatically cleaved to peptides before measurements via tandem MS; top-down MS targets intact proteins rather than peptides for analysis, with the aim to define the protein primary structure by providing highly accurate structural assignment of MS/MS fragments. In this way, we obtained a detailed overview of the proteins in the isolated PSII–LHCII supercomplexes of different organization, revealing the presence of the antenna proteins Lhcb3 and Lhcb6 and of the extrinsic polypeptides PsbP, PsbQ and PsbR exclusively in the $C_2S_2M_2$ supercomplex. Other proteins of the PSII core complex, common to the $C_2S_2M_2$ and $C_2S_2$ supercomplexes, including the LMM subunits, were also detected and characterized. Conversely, the LHCII-like PsbS protein was not detected in either the $C_2S_2M_2$ or $C_2S_2$ supercomplex.

To date, the only 3D structure available of a PSII–LHCII supercomplex has been obtained at 17 Å resolution by cryo-transmission electron microscopy (cryo-TEM) and single particle analysis of $C_2S_2$ isolated particles containing only one LHCII trimer (S-trimer) per RC core and lacking the minor antenna Lhcb6 [18–20]. For the supercomplex of type $C_2S_2M_2$ only 2D projection maps obtained by TEM analysis of negatively stained single particles derived either from fully or partially solubilized thylakoids are available [15–17,21]. In this paper we show 3D electron density maps, derived from negatively stained samples, for the $C_2S_2M_2$ supercomplex as well as for its $C_2S_2$ subcomplex from pea (*Pisum sativum*), with resolutions respectively of 30 and 28 Å, subsequently extended by molecular modelling towards atomic level.

## 2. Material and methods

### 2.1. PSII–LHCII supercomplexes isolation

Stacked thylakoid membranes were isolated from pea plants according to [22]. By solubilizing thylakoid membranes either with α-DM or β-DM, followed by sucrose density gradient ultracentrifugation, PSII–LHCII supercomplexes of different size were isolated, attributable to the $C_2S_2M_2$ and $C_2S_2$ organization, respectively, as described in our previous paper [17]. Sucrose bands, containing PSII–LHCII supercomplexes, were carefully removed using a syringe and, if necessary, concentrated by membrane filtration with Amicon Ultra 100 kDa cut-off devices (Millipore) and then stored at −80 °C. The Chl concentration was determined spectrophotometrically after extraction in 80% (v/v) acetone according to [23].

### 2.2. Gel electrophoresis and western blotting

PSII–LHCII supercomplexes were analysed in native conditions by using the blue-native polyacrylamide gel electrophoresis (BN-PAGE) system according to [24], with a 3–12% acrylamide separating gel and a 4% acrylamide stacking gel. Prior to loading, samples were supplemented with a one-sixteenth volume of the loading buffer (750 mM ε-amino caproic acid, 5% (w/v) Coomassie G250) and incubated for 10 min on ice. After centrifugation at 21,000 ×*g* for 10 min, the supernatants were loaded onto the 20 cm gradient gel and run for 7 h at a constant voltage of 70 V, using as anode buffer a solution made of 50 mM Bis-Tris–HCl pH 7.0 and as cathode buffer a solution made of 50 mM Tricine, 15 mM Bis-Tris–HCl pH 7.0, and 0.02% (w/v) Coomassie G250. After two-thirds of the run, the cathode buffer containing Coomassie G250 was replaced by a buffer with the same composition but devoid of Coomassie G250 and run overnight at a constant voltage of 60 V. For molecular mass markers, a mixture of lyophilized standard proteins (Amersham, high molecular mass calibration kit (code 17-0445-01), GE Healthcare) was used. For bi-dimensional sodium dodecyl sulphate polyacrylamide gel electrophoresis (2D SDS-PAGE), bands corresponding to $C_2S_2M_2$ and $C_2S_2$ PSII–LHCII supercomplexes resolved on BN-PAGE were cut out and equilibrated in a buffer made of 66 mM $Na_2CO_3$, 2% (w/v) SDS and 0.66% (v/v) 2-mercaptoethanol at 25 °C for 30 min and subjected to 15% acrylamide SDS-PAGE containing 6 M urea using Laemmli's system [25].

Mono-dimensional sodium dodecyl sulphate polyacrylamide gel electrophoresis (1D SDS-PAGE) was performed on a linear gradient gel (18–22% acrylamide) containing 6 M urea using Kashino et al.'s system [26], to improve the resolution of LMM subunits.

The proteins separated in 1D or 2D SDS-PAGEs were either stained by 0.25% (w/v) Coomassie R250 for 1 h in a solution made of 50% (v/v) methanol and 10% (v/v) acetic acid, and destained by a solution made of 25% (v/v) methanol and 7.5% (v/v) acetic acid, or transferred onto nitro-cellulose membrane and immunodetected with a specific antiserum (Agrisera, catalog number AS09533) against the

PsbS polypeptide, by using the alkaline phosphatase conjugate method, with 5-bromo-4-chloro-3-indolyl phosphate/nitro blue tetrazolium as chromogenic substrates (Sigma-Aldrich).

### 2.3. Mass spectrometry

For liquid nano chromatography electrospray ionization tandem mass spectrometry (nanoLC-ESI-MS/MS) analysis, spots from the 2D SDS-PAGE and bands from the 1D SDS-PAGE were cut out and proteins were digested in-gel with trypsin (Roche), as described in Hellmann et al. [27]. NanoLC-ESI-MS/MS data from each protein sample were obtained by using a Q-star XL (AB SCIEX) as previously described [28]. Mascot.dll v 1.4804.0.22 (Matrix Science/AB SCIEX) was used to generate Mascot (.mgf) files with peak lists from the Analyst QS 2.0 (.wiff) files. The MS/MS spectra, that were obtained using digested samples, were analysed as Mascot generic files against all entries in the public NCBInr database using the online Mascot server (Matrix Science: http://www.matrixscience.com/) without a taxonomy filter.

The principal parameter settings for the Mascot search were as follows: database NCBInr (version 2012.02.26; containing 17,406,376 sequence entries); enzyme trypsin; allow up to one missed cleavage; possible variable modifications carbamidomethylation of cysteine (C), oxidation of methionine (M), deamidation of asparagine and glutamine (NQ); precursor ion mass and fragment masses tolerance respectively of 60 ppm and 0.3 Da; instrument ESI-QUAD-TOF; default charge state set to 2+, 3+, and 4+. Widely accepted procedures for positive identifications of proteins by MS/MS analysis require a minimum of two unique peptides with at least one peptide having a significant ion score ($p \leq 0.05$). Considering that the genome of *P. sativum* is not fully sequenced, and that only some protein sequences of *P. sativum* are present in the database, we also accepted, as confident assignments, hits identified by at least one peptide with a significant ion score according to the MASCOT MS/MS ion search algorithm.

For matrix-assisted laser desorption/ionization-time of flight (MALDI-TOF) and matrix-assisted laser desorption/ionization-time of flight/time of flight (MALDI-TOF/TOF) MS analyses, the isolated PSII–LHCII supercomplexes were initially dialyzed for 18 h against 5% (v/v) acetic acid, using a 12–14 kDa cut-off membrane (Spectra/Por, SpectrumLabs), and further concentrated to 1/10 of the initial volume by membrane filtration with Amicon Ultra 100 kDa cut-off devices (Millipore). 1 μl of each concentrated sample was mixed with 9 μl of saturated matrix (sinapic acid, Laser Biolabs) solution which consists of 60% (v/v) acetonitrile and 0.1% (v/v) trifluoroacetic acid. After drying droplets of sample onto a target plate, MALDI-TOF and MALDI-TOF/TOF MS analyses were performed using respectively the mass spectrometers Voyager-DE PRO MALDI-TOF (AB SCIEX) and MALDI-TOF/TOF™ 5800 System (AB SCIEX).

The MALDI-TOF mass spectrometer was operated in linear mode at 25 keV accelerating voltage, grid 96.5%, guide wire 0.05% and 800 ns ion extraction delay; the nitrogen laser working at 337 nm and 3 Hz. Two hundred laser shots were accumulated per spectrum over an *m/z* range of 3500–10,000. Internal calibration was performed on the samples premixed with Calibration mixture 2 of the Peptide Mass Standards Kit for Calibration of AB SCIEX MALDI-TOF Instruments.

MALDI TOF-TOF spectra were acquired using the AB SCIEX TOF/TOF ™ 5800 system operated with positive ionization either in linear mode, to determine the average molecular mass, or in reflector mode, to analyse the fragments. An internal calibration was performed on the samples premixed with polyethylene glycol (PEG4000). MS/MS was carried out on the top precursors. Between twenty thousand and two hundred thousand shots were accumulated to get the best S/N, with laser frequency of 1 kHz, acceleration voltage of 2 keV and using air as collision gas. The MS/MS spectra, obtained from the main proteins peaks in MS, were analysed in Mascot Distiller (ver. 2.3.2.0) by the *de novo* sequencing function coupled with MS-Blast (http://dove.embl.de/Blast2/msblast.html) search at EMBL http://www.embl.de/ [29], using default parameter values.

### 2.4. Transmission electron microscopy and 3D single particle image analysis

PSII–LHCII supercomplexes isolated with α-DM were negatively stained with 2% uranyl acetate, as described previously [17], and imaged at a calibrated magnification of 50,000× and an acceleration voltage of 200 keV with a Philips CM200 transmission electron microscope equipped with a field emission gun (FEG) at the Electron Microscopy Centre, Imperial College London, UK. A total of 600 CCD images were recorded under low dose conditions (electron dose of approximately 20 electrons/Å$^2$) on a 4096 × 4096 15 μm/pixel slow-scan CCD camera TemCam-F415MP (TVIPS, Germany), leading to a final pixel size corresponding to 1.76 Å at the specimen level. Imaging conditions were optimised, in terms of defocus and astigmatism, to ensure the first minima of the power spectrum to be within a range of 10 to 25 Å, equivalent to an underfocus range of 0.5 to 1.5 μm. Particles were floated out into boxes using EMAN2 [30]. All subsequent image processing was performed within the IMAGIC-V software (Imagic Science, Berlin, Germany) environment [31], at a sampling frequency of 7.04 Å per pixel, until the final reference-free alignment [32] iteration reverted back to 1.76 Å per pixel. A dataset of 15,563 negatively stained single particle images were obtained by picking all discernible single particles present. Several sub-populations of particles, differing in size and shape, were identified. The two largest sub-populations, corresponding to the $C_2S_2M_2$ and the $C_2S_2$ PSII–LHCII supercomplexes, were in turn analysed as separate datasets, with the reference free alignment giving the initial class averages necessary for multi-reference alignment. Relative orientations were determined for the class averages by the angular reconstitution technique [33] and initial 3D reconstructions gained from implementation of the exact back projection technique [34]. Reprojections were taken from each 3D model and used to identify additional atypical views and further refine the class averages within each sub-population dataset. Through iterative refinement the data converged to give the best 3D reconstructions shown. Resolution was determined by calculating the Fourier shell correlation (FSC) at the 3σ criterion between two independent 3D reconstructions [35]. Relevant crystallographic co-ordinate atom data (PDB identifiers: 3ARC, 2BHW, 3PL9) were modelled into molecular maps derived from the sub-populations using PyMOL (The PyMOL Molecular Graphics System, Version 1.1r1, Schrödinger, LLC) and UCSF Chimera [36] modelling software. Surface rendered views were calculated at a threshold of 2.5 σ.

## 3. Results and discussion

### 3.1. Different protein composition of PSII–LHCII supercomplexes of types $C_2S_2M_2$ and $C_2S_2$

PSII–LHCII supercomplexes isolated from pea thylakoid membranes solubilized with α- or β-DM, and shown previously to be of types $C_2S_2M_2$ and $C_2S_2$ respectively [17], were extensively subjected to in-depth proteomic analyses in order to detect specific proteins (*i.e.*, peripheral antenna proteins, extrinsic polypeptides, and LMM subunits) that may be related to the presence of the additional LHCII M-trimers associated with the $C_2S_2$ basic supercomplex of PSII.

To investigate the association of the LHCII proteins with the dimeric PSII core complex, in the two differently isolated PSII–LHCII supercomplexes, BN-PAGE followed by 2D SDS-PAGE, coupled with nanoLC-ESI-MS/MS analysis, were performed. In Fig. 1A the BN-PAGE profile of the PSII–LHCII supercomplexes isolated from pea thylakoid membranes solubilized with α-DM (lane 1) and β-DM (lane 2) shows, in the former case, a predominant green band, attributable to the $C_2S_2M_2$ supercomplex, with a higher molecular mass with respect to that of the band observed in the latter, and attributable to the $C_2S_2$ supercomplex. The difference in mass (~300 kDa) between these two

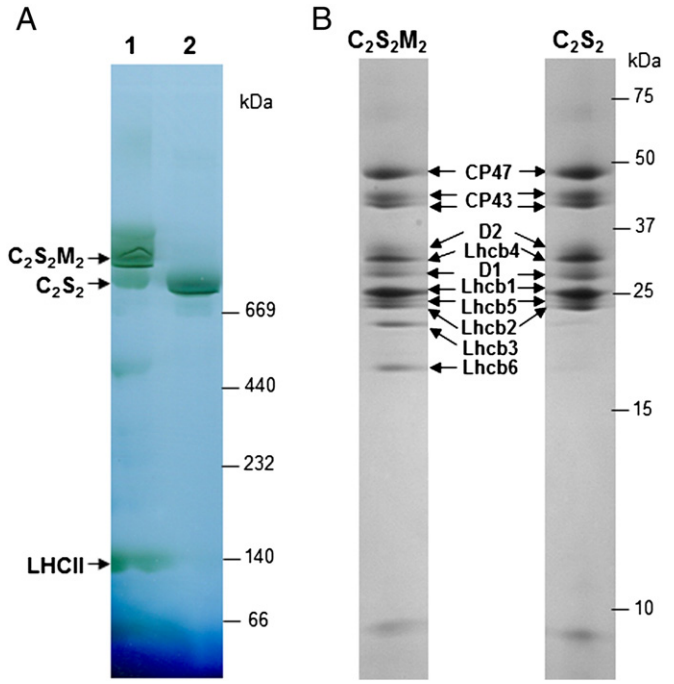


**Fig. 1.** BN/2D SDS-PAGE profiles of PSII–LHCII supercomplexes isolated from pea thylakoid membranes. A. BN-PAGE of PSII–LHCII supercomplexes isolated from pea thylakoid membranes solubilized with α-DM (lane 1) and β-DM (lane 2) (6 μg Chl per lane). Protein marker (native high molecular mass, GE Healthcare) positions indicated on the right. B. 2D SDS-PAGE separation of $C_2S_2M_2$ and $C_2S_2$ supercomplexes, after Coomassie staining. Protein marker (Precision plus, Bio-Rad) positions indicated on the right.

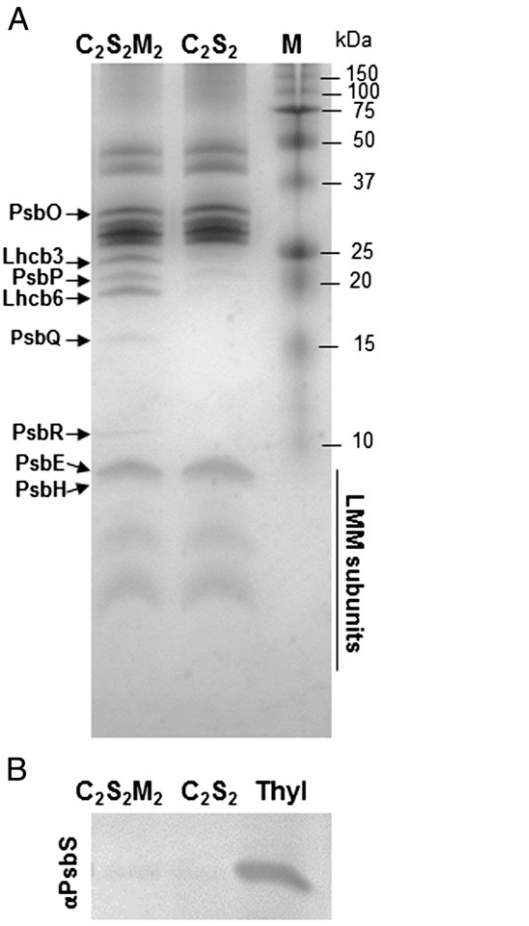


**Fig. 2.** 1D SDS-PAGE and western blot analysis of PSII–LHCII supercomplexes isolated from pea thylakoid membranes. A. Profiles of protein composition of $C_2S_2M_2$ and $C_2S_2$ supercomplexes (10 μg Chl per lane) resolved by 1D SDS-PAGE according to [26]. Protein standards (Precision plus, Bio-Rad) are loaded on lane M. B. Western blot analysis using the antibody against PsbS. Pea thylakoid membranes (Thyl) loaded as control (10 μg Chl on each lane).

bands is indicative of the retention, by the $C_2S_2M_2$ supercomplex, of two additional LHCII M-trimers. The two green bands corresponding to the $C_2S_2M_2$ and $C_2S_2$ supercomplexes were cut out from the native gel and subsequently separated by denaturing 2D SDS-PAGE, whose profile, after Coomassie staining, shows the two corresponding maps of spots derived from their membrane polypeptide components (Fig. 1B). After in-gel trypsin digestion of all the spots, nanoLC-ESI-MS/MS analysis of the digested peptides revealed the identity of the RC core subunits CP47, CP43, D2 and D1, and of the six Lhcb antenna proteins (Lhcb1-6) (Table S1), allowing their positioning on the 2D SDS-PAGE maps to be identified (Fig. 1B). From these analyses, it was found that the antenna proteins Lhcb3 and Lhcb6 are present only in the $C_2S_2M_2$ supercomplex with the Lhcb3 being exclusively located in the LHCII M-trimer, together with Lcb1 and Lhcb2 [16], and the Lhcb6 functioning as a linker for this trimer to the $C_2S_2$ supercomplex [15,17].

In lane 1 of Fig. 1A, however, two additional faint bands were detected below the predominant one: the one with higher molecular mass corresponds to $C_2S_2$ supercomplexes and the second, with lower molecular mass (~150 kDa), to free trimers of LHCII. Despite care taken during the PSII–LHCII isolation process, the presence of these complexes in the preparation obtained with α-DM indicates a degree of instability of the isolated $C_2S_2M_2$ supercomplex and the easy detachment of LHCII M-trimers from the $C_2S_2M_2$ supercomplex.

In order to determine the exact protein composition of the $C_2S_2M_2$ and $C_2S_2$ supercomplexes, also in terms of extrinsic polypeptides and LMM subunits, we performed a separation of their proteins in 1D SDS-PAGE according to the system of Kashino et al. [26], shown in Fig. 2A. This electrophoretic system, in combination with nanoLC-ESI-MS/MS analysis (as for proteins separated through 2D SDS-PAGE), allowed the detection and identification of the extrinsic polypeptides PsbO, PsbP, PsbQ and PsbR (Table S1, Fig. 2A). The level of PsbO appeared to be less sensitive, compared to the other OEC subunits, to perturbation during the solubilization with both forms of DM. The relative stability of PsbO in both isolated PSII–LHCII supercomplexes is due to the interaction of its N-terminal region with several PSII RC subunits, including CP47, CP43, D1 and D2, as shown in the cyanobacterial crystal structure [37–39]. Moreover, numerous cross-linking studies have indicated that the PsbO protein may be cross-linked to CP47 in higher plants [40–42]. The milder action of α-DM as the solubilizing agent also facilitated the partial retention of the extrinsic subunits PsbP, PsbQ and PsbR in the $C_2S_2M_2$ supercomplex. These polypeptides were not present in the $C_2S_2$ supercomplex, indicating that they are not absolutely required to stabilize the binding of LHCII S-trimers to the PSII RC core. This partial retention may reflect heterogeneity in the band of the sucrose gradient containing the $C_2S_2M_2$ supercomplex (as indicated also by electron microscopy, see below), which in turn could be in part due to differential detergent effects associated with the purification procedure. Of note is the fact that, in addition to the PsbQ protein, in the isolated $C_2S_2M_2$ supercomplex the PsbP and PsbR extrinsic subunits were detected. These two proteins were not found in a similar preparation obtained from the thylakoid membranes of *A. thaliana* solubilized with α-DM by Caffarri et al. [15]. Interestingly, recent studies have shown important roles played by the PsbP, PsbQ and PsbR subunits in PSII–LHCII supercomplex macro-organization and stabilization [43,44].

The Lhcb-like PsbS protein seems to play a role in the distribution of light to the PSII RC by regulating non-photochemical quenching [45]. It has been argued that it does so by controlling PSII–LHCII supercomplex macro-organization [46]. Our MS analyses did not reveal the presence of this protein in either isolated $C_2S_2M_2$ or $C_2S_2$ supercomplexes, in agreement with previous reports [15,47]. As this protein is believed to be present in non-stoichiometric amounts compared with other PSII

proteins, we undertook a sensitive immunological analysis using an antibody with strong reactivity to PsbS in pea thylakoid membranes. This analysis did not detect the PsbS protein in any of the isolated supercomplexes (Fig. 2B), and showed that the protein co-migrated with the free LHCII band in the sucrose density gradient step adopted in the isolation of supercomplexes (data not shown). This finding contrasts with that of Caffarri et al. [15], who concluded that PsbS co-migrated with the $C_2S_2M_2$ supercomplex in their sucrose density gradient.

### 3.2. Common content in LMM subunits in PSII–LHCII supercomplexes of types $C_2S_2M_2$ and $C_2S_2$

The high resolution of Kashino's electrophoretic system [26], especially appropriate for the low molecular masses, allowed for the separation of the LMM subunits present in the $C_2S_2M_2$ and $C_2S_2$PSII–LHCII supercomplexes. After in-gel trypsin digestion of all bands with masses <10 kDa, nanoLC-ESI-MS/MS analysis of the digested peptides revealed the presence of PsbE and PsbH (Table S1, Fig. 2A) in both supercomplexes, but failed to detect PSII components with lower molecular masses. This was likely due to the higher hydrophobicity of these transmembrane proteins, almost completely embedded in the membrane, due to their short length, which lowers the accessibility of trypsin enzyme and the number of tryptic cleavage sites present in their sequences. On the contrary, by applying MALDI-TOF and MALDI-TOF/TOF MS directly to the isolated $C_2S_2M_2$ and $C_2S_2$ supercomplexes, it was possible to identify most of the expected LMM subunits present in the two samples: PsbX, PsbTc, PsbJ, PsbI, PsbK, PsbL, PsbF, PsbW, and PsbE (Fig. 3, Table 1).

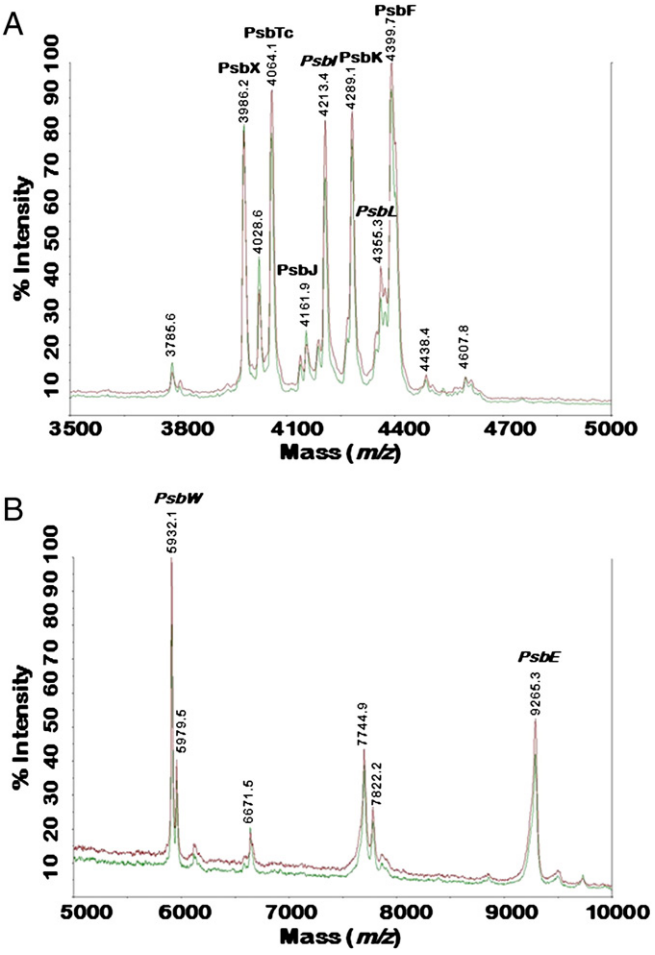


**Fig. 3.** MALDI-TOF mass spectra of PSII–LHCII supercomplexes of type $C_2S_2M_2$ (green line) and $C_2S_2$ (red line) isolated from pea thylakoid membranes. A. Peaks with *m/z* values between 3500–5000. B. Peaks with *m/z* values between 5000–10,000. Denoted above the peaks, names of proteins in bold refer to LMM subunits identified by MS/MS analysis and *de novo* sequencing (see Table S2), those in italics refer to putative assignments based on good correlation between observed *m/z* and referenced values for masses measured on isolated LMM subunits from pea, spinach and barley [48–50].

It is worth noting that MALDI-TOF measurements performed on three independent preparations of $C_2S_2M_2$ and $C_2S_2$ supercomplexes were highly reproducible, and that in both types of samples corresponding peaks were observed at coincident *m/z* values, given a mass tolerance of 50 ppm (the MALDI TOF technique is accurate to a 100 to 50 ppm average error, achieved by internal calibration). The overlapping of MALDI-TOF mass spectra for the $C_2S_2M_2$ and $C_2S_2$ samples in the range of *m/z* below 10,000 confirmed the common composition in LMM subunits of the two isolated supercomplexes (Fig. 3). In this range of *m/z*, several peaks were detected, most of which have been identified as follows: 3986.2 ± 0.2 as PsbX, 4064.1 ± 0.2 as PsbTc, 4161.9 ± 0.2 as PsbJ, 4213.4 ± 0.2 as PsbI, 4289.1 ± 0.2 as PsbK, 4355.3 ± 0.2 as PsbL, 4399.7 ± 0.2 as PsbF, 5932.1 ± 0.3 as PsbW, 9265.3 ± 0.5 as PsbE (Fig. 3, Table 1).

The identification of the proteins PsbX, PsbTc, PsbJ, PsbK and PsbF was assigned by MS/MS analysis on the corresponding selected precursor main peaks combined with *de novo* sequencing and homology searching (see Table S2, and Figs. S1–S5). Among these five assignments:

1) the observed *m/z* values for PsbK and PsbF are in good agreement with *m/z* values measured on these isolated proteins from pea, spinach and barley [48–50], and also with expected molecular masses calculated from the corresponding genomic sequences from pea, taking into account, in the case of PsbF, the Met1 removal and Thr2 acetylation suggested as post translational modifications (PTMs) by Sharma et al. [48];
2) the observed *m/z* value obtained for PsbTc is respectively higher than that measured for this protein isolated from spinach by Zheleva et al. [49] and lower than that experimentally found for its homolog from barley by Plöscher et al. [50]. This can be explained by the different length of the protein sequence among the three plants: 35 amino acid residues in pea, 33 in spinach and 38 in barley (accession numbers in the UniProtKB database: Q8HS25, P61840 and P69669, respectively). Moreover, the mass difference between the observed value and that expected from the calculated corresponding genomic sequence from pea, could indicate a formyl-methylation as PTM, as found for this protein in spinach by Zheleva et al. [49];
3) in the literature there are measured values of *m/z* for PsbX and PsbJ proteins purified only from barley for comparison [50]. The observed value of *m/z* for PsbJ is higher than that measured for its homolog in barley. Despite the same length of the protein sequence in pea and barley, the different *m/z* value observed in the two plants can be explained by the presence of five amino acid substitutions (Asn3 *vs* Asp3, Ile12 *vs* Leu12, Val20 *vs* Pro20, Ile25 *vs* Val25, Leu27 *vs* Val27) in the sequence from pea with respect to barley (accession numbers in the UniProtKB database: P13555 and P20175, respectively). The *m/z* value observed for PsbJ closely matches the expected mass calculated from the corresponding genomic sequence, with a slight difference possibly linked to an N-acetylation suggested as PTM by Plöscher et al. [50] in barley. In the case of PsbX, the experimental *m/z*, that is slightly lower than that measured for its homolog in barley, accounts for less than a half of the expected mass calculated from its genomic sequence and the sequence obtained by *de novo* sequencing for this protein covers the C-term portion of the amino acid sequence present in the UniProtKB database (Tables 1 and S2).

The putative assignment of PsbI, PsbL, PsbW and PsbE was done by comparing the experimental *m/z* measured by MALDI-TOF either with results obtained by ESI MS/MS and/or MALDI-TOF MS and N-terminal

**Table 1**
Proposed identification of measured *m/z* peaks in PSII–LHCII supercomplexes of types $C_2S_2M_2$ and $C_2S_2$ isolated from pea thylakoid membranes. The table reports the reproducible *m/z* values measured by MALDI-TOF (first column) on three independent preparations of $C_2S_2M_2$ and $C_2S_2$ supercomplexes (similar values for both types of samples were obtained. See text for details and Fig. 3), assigned by *de novo* sequencing and homology searching (second column) on MS/MS data (see Table S2 and Figs. S1–S5), or putatively assigned (third column) according to matches with referenced values (fourth column). For each identified subunit, expected mass values of unprocessed precursors and processed proteins (sequences from UniProtKB-Swiss Prot), including annotated PTMs, are reported (fifth column), along with referenced masses and corresponding organisms (*Hordeum vulgare*, *Spinacia oleracea*, *Pisum sativum*), when available (fourth column).

| Observed *m/z* | *De novo* sequencing assignment | Putative assignment | Referenced *m/z*, organism | Calculated average molecular mass of unprocessed precursor/accession UniProtKB (*P. sativum* or *S. oleracea*)/ annotated PTMs (calculated average molecular mass of processed precursor) |
|---|---|---|---|---|
| 3986.2 ± 0.2 | *PsbX* | | 4141.32 [50], *H. vulgare* | 8683.1/Q8VYY1 (*P. sativum*) |
| 4064.1 ± 0.2 | *PsbTc* | | 3849.6 [49], *S. oleracea*; 4422.05 [50], *H. vulgare* | 4032.9/Q8HS25 (*P. sativum*) |
| 4161.9 ± 0.2 | *PsbJ* | | 4011.15 [50], *H. vulgare* | 4115.9/P13555 (*P. sativum*) |
| 4213.4 ± 0.2 | | *PsbI* | 4209.5 [48], *P. sativum*; 4195.5 [49], *S. oleracea*; 4193.28 [50], *H. vulgare* | 4182.0/D5MAJ9 (*P. sativum*)/N-formyl Met (4210.0) |
| 4289.1 ± 0.2 | *PsbK* | | 4292.1 [49], *S. oleracea;* 4282.40 [50], *H. vulgare* | 6910.4/D5MAJ8 (*P. sativum*)/N-term 1–24 removed (4285.2) |
| 4355.3 ± 0.2 | | *PsbL* | 4365.5 [49], *S. oleracea;* 4363.17 [50], *H. vulgare* | 4497.2/P60147 (*P. sativum*) |
| 4399.7 ± 0.2 | *PsbF* | | 4394.6 [48], *P. sativum*; 4409.1 [49], *S. oleracea;* 4406.40 [50], *H. vulgare* | 4424.3/P62096 (*P. sativum*) |
| 5932.1 ± 0.3 | | *PsbW* | 5927.4 [49], *S. oleracea;* 5889.00 [50], *H. vulgare* | 14177.2/Q41387 (*S. oleracea*)/N-term 1–83 removed (5927.7) |
| 9265.3 ± 0.5 | | *PsbE* | 9283.6 [48], *P. sativum*; 9255.1 [49], *S. oleracea;* 9307.83 [50], *H. vulgare* | 9414.6/P13554 (*P. sativum*)/Met1 removed (9283.4) |

amino acid sequencing present in the literature for these LMM subunits purified from higher plants [48–50], or with protein masses calculated from the corresponding nucleotide sequences from pea (Table 1). For PsbI, PsbW and PsbE both correlations were good; in case of PsbL, the measured *m/z* closely matched that obtained for this subunit in spinach and barley [49,50], and the difference observed between the measured and the expected molecular mass calculated from its genomic sequence from pea, can be likely due to the Met1 removal, a PTM found in its corresponding analog in spinach and barley [49,50].

Despite the reproducible signal strength of peaks at *m/z* 4028.6 ± 0.2 and 7744.9 ± 0.4, it was not possible to assign a specific identity to these masses by MS/MS. However, the measured *m/z* value at 7744.9 can be tentatively assigned to PsbH, due to the identification of this subunit by nanoLC-ESI-MS/MS analysis in both PSII–LHCII supercomplexes (Table S1, Fig. 2A), and the good correlation between the measured mass and the expected molecular mass calculated from its genomic sequence in *P. sativum* (accession number in the UniProtKB database Q9XQR3, calculated average mass after Met1 removal 7726.95).

### *3.3. 3D reconstructions of the PSII–LHCII supercomplexes of types $C_2S_2M_2$ and $C_2S_2$ revealed by TEM single particle analysis and angular reconstitution*

Negative stain TEM from the sucrose density gradient fraction containing PSII–LHCII supercomplexes obtained by solubilizing pea thylakoid membranes with α-DM provided for a single particle dataset of 15,563 images, as described previously [17]. In the current study, this dataset was re-subjected to more intensive computer-based purification analyses, so that more rigorously defined sub-populations of particles might be identified prior to the application of the 3D reconstruction technique of angular reconstitution [34]. In so doing, sub-populations of 4760 and 1868 particles were identified relating to the largest complexes, in terms of surface area with two-fold symmetry. These were attributed to the $C_2S_2M_2$ and $C_2S_2$ PSII–LHCII supercomplexes respectively. Following *de novo* reference-free alignments, the relative angular orientations of the particles observed within each sub-population were strongly biased towards top and side views; however, subsequent iterative refinements were able to identify a small amount of slightly tilted views which aided in the calculation of the final 3D electron density maps.

In Fig. 4A the 3D electron density map of the $C_2S_2M_2$ supercomplex is represented in green mesh as viewed from the top lumenal side and the $C_2S_2$ 3D electron density map has been incorporated within, surface-rendered in light blue. The $C_2S_2M_2$ map has a maximum dimension of 375 Å length by 210 Å width by 105 Å height, with a two-fold axis and an approximate resolution of 30 Å. The $C_2S_2$ map is also shown with two-fold imposed symmetry, having a dimension of 340 Å length by 200 Å width by 105 Å height with a resolution approaching 28 Å. To interpret these 3D electron density maps, we compared their internal density distribution with surface-rendered X-ray structures (see Fig. 4B) of the PSII dimeric core of cyanobacteria at 1.9 Å [39], the LHCII trimeric complex of pea at 2.5 Å [11] and the monomeric Lhcb4 of spinach at 2.8 Å [12]. The latter was extrapolated to represent densities we attributed previously to the Lhcb5 and Lhcb6 subunits [17], whose X-ray structures have yet to be solved. Modelling the co-ordinates within the two molecular envelopes was done by visual inspection using the internal densities (not shown) as a guide, starting centrally with the $C_2S_2$ model of Nield and Barber [20], treated as a rigid whole, and extending out to include two Lhcb6 subunits and two LHCII M-trimers. In the 3D map of the $C_2S_2M_2$ supercomplex the location of the additional LHCII M-trimers is peripheral relative to the LHCII S-trimers, while the positioning of Lhcb6 adjacent to Lhcb4 is supported by experimental findings showing that the five-subunits membrane complex, composed of Lhcb4, Lhcb6 and LHCII M-trimer, can easily be detached from the $C_2S_2M_2$ supercomplex under high light conditions [51,52]. The entire modelling environment encompassed a depth of 130 Å and this thickness is shown in full in Fig. 4A–B. The cyanobacterial PSII dimeric core X-ray co-ordinates (excluding those of PsbV and PsbU), when shown surface-rendered (Fig. 4B), are able to emphasise the key differences between the cyanobacterial lumenal surface and our molecular envelopes from pea. However, the prevalence of top and side views, coupled with the availability of only a few tilted views, due to the negative stain methodology employed, was found in this particular work to suppress the density expected for the lumenally-exposed polypeptides of the OEC and therefore limit our maps' interpretability in this regard. Reducing the slabbed area to 65 Å in Fig. 4C–D enabled the visualisation of the entire membrane domain, the interactions between the LHCII antennae proteins with specific subunits of the PSII core complex and the relative overall positioning of the additional LHCII M-trimers and the Lhcb6 subunits present in the $C_2S_2M_2$ supercomplex (the latter two in 1:1 stoichiometry with the PSII monomeric core which they bind). In Fig. 4D the $C_2S_2$ map was removed from the modelling environment and, noting an approximate 10 Å wide boundary for the detergent shell (yellow line) encompassing the TEM-derived $C_2S_2M_2$ green mesh, the major domains of the largest PSII–LHCII supercomplex we observed in α-DM solubilized pea thylakoids can be interpreted more readily.

## 4. Conclusions

By means of bottom-up and top-down MS we have conducted an in-depth characterization of the polypeptide composition of PSII–LHCII supercomplexes of types $C_2S_2M_2$ and $C_2S_2$ isolated from pea thylakoid

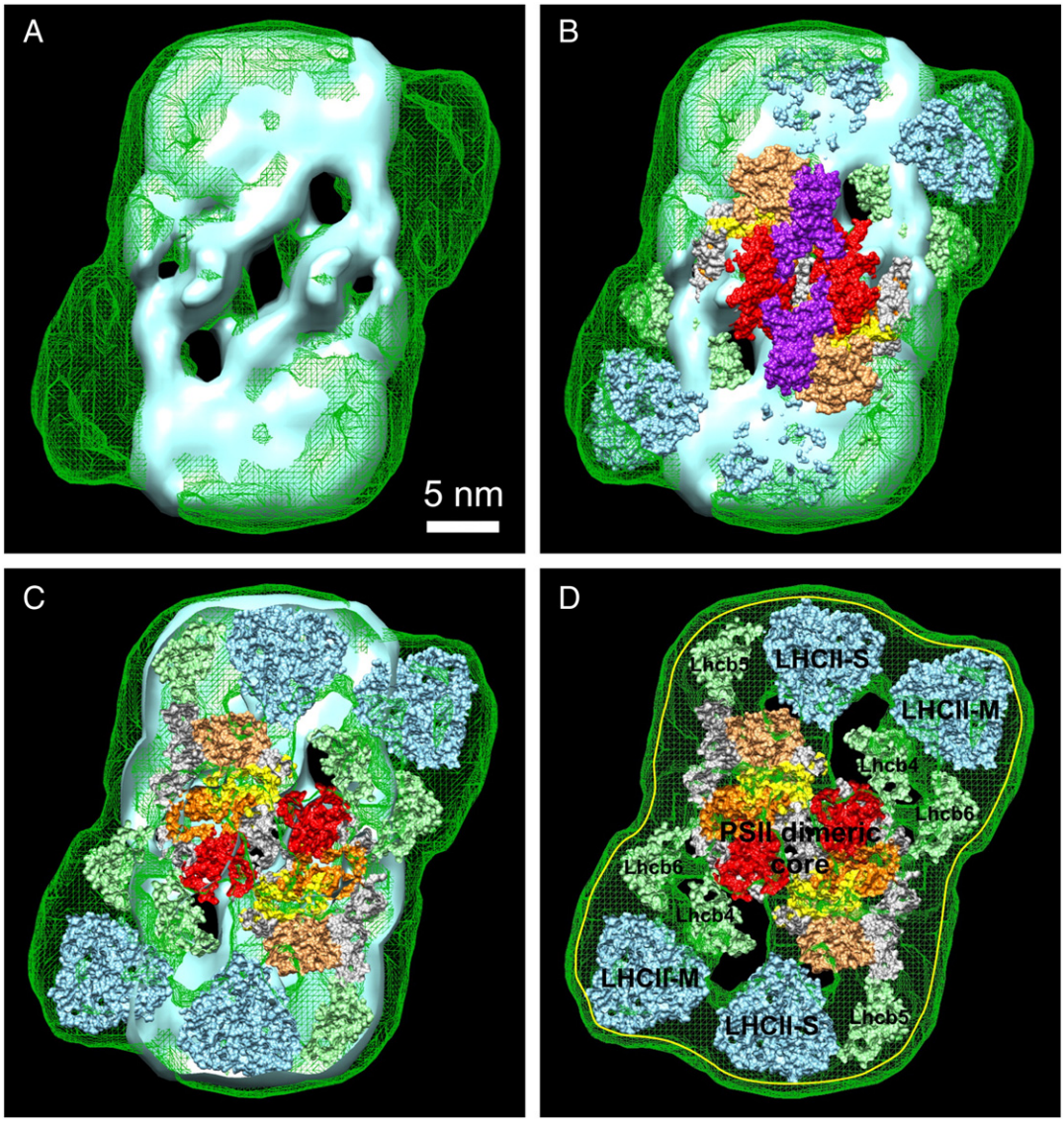


**Fig. 4.** Top lumenal views of 3D reconstructions of the $C_2S_2M_2$ and $C_2S_2$ PSII–LHCII supercomplexes isolated from pea thylakoid membranes, derived from TEM and single particle analysis, with modelled high-resolution X-ray structures of the PSII dimeric core from cyanobacteria [39] (PDB ID: 3ARC; subunits D1, D2, CP47, CP43 and PsbO are in yellow, orange, red, sandy brown and purple, other subunits in grey, respectively; PsbU and PsbV have been omitted from the PDB file), the LHCII trimer [11] (PDB ID: 2BHW; in blue) and Lhcb4 [12] (PDB ID: 3PL9; in pale green), the latter two from higher plants. A. Top lumenal view of the $C_2S_2M_2$ 3D electron density map (green mesh), with the $C_2S_2$ 3D electron density map, inset, surface-rendered in light blue. Maximum dimensions (in plane) of the 3D maps, inclusive of the detergent shell, are 375 Å (length) × 210 Å (width) for $C_2S_2M_2$ and 340 Å (length) × 200 Å (width) for $C_2S_2$ supercomplexes. Scale bar for all panels represents 5 nm. B. As per panel A, with the cyanobacterial PSII dimeric core present, highlighting lumenal surface differences, together with LHCII trimer and monomeric Lhcb atomic co-ordinates shown as surface-rendered spheres (coloured as described above). C. The modelling environment, cut away by 65 Å, to reveal its lower half, also 65 Å thick, thus emphasising the position of the X-ray co-ordinates (surface-rendered and coloured as described above). D. The $C_2S_2M_2$ 3D cut away map (as in C) on its own with modelled subunits labelled (surface-rendered and coloured as described above), its membrane domain also shown as a 65 Å thick slab from the lumenal top view. The Lhcb5 and Lhcb6 atomic co-ordinates, whose structures have not yet been solved, are assumed to be similar to that of Lhcb4. A delineating boundary (yellow line) represents the α-DM detergent shell, approximately 10 Å within the outer edge of the $C_2S_2M_2$ three-dimensional mesh.

membranes by one-step treatment with α- and β-DM detergents, respectively, as described previously [17]. Their protein composition, spanning from RC and LMM intrinsic subunits to antennae proteins and extrinsic polypeptides, was revealed. In addition to a common composition in the main PSII RC proteins, the $C_2S_2M_2$ and $C_2S_2$ supercomplexes showed an identical set of LMM subunits. Thus, we conclude that among the identified LMM subunits none is specifically required for the binding of the additional LHCII M-trimers to the basic $C_2S_2$ unit. In contrast to the LMM subunits, the two isolated supercomplexes revealed basic differences in their Lhcb antennae polypeptides: Lhcb1, Lhcb2, Lhcb4 and Lhcb5 were found in both the $C_2S_2M_2$ and $C_2S_2$ supercomplexes, whereas Lhcb3 and Lhcb6 were present only in the largest supercomplex, suggesting that Lhcb3 is exclusively located in the LHCII M-trimer and Lhcb6 functions as a linker for this LHCII trimer to the $C_2S_2$. The Lhcb-like PsbS protein was not found to be associated with the isolated supercomplexes, indicating that this subunit does not influence the interaction between the PSII core and the outer Lhcb antenna system. Due to the high hydrophobicity of this protein, its absence from the isolated supercomplexes and abundance in the free LHCII trimers (LHCII band in the sucrose density gradient adopted in the isolation of supercomplexes), suggests that its location is in the peripheral boundary of the PSII–LHCII supercomplexes or in the LHCII-enriched domains of the thylakoid membranes. The proteomic data indicate that, in addition to the PsbO subunit, which is stably

bound to the PSII RC core in both types of supercomplexes, the $C_2S_2M_2$ supercomplex retains partially the PsbP, PsbQ and PsbR subunits.

A pseudo-atomic 3D structural model of the spinach $C_2S_2$ supercomplex, based upon a cryo-TEM molecular envelope calculated at 17 Å resolution, was previously reported by Nield and Barber [20]. However, for the larger $C_2S_2M_2$ supercomplex, only 2D projection maps obtained by TEM of negatively stained single particles have been published to date [15–17,21].

Here we report the first 3D structural model of an isolated $C_2S_2M_2$ supercomplex obtained by single particle analysis of negatively stained samples as imaged by TEM. The resolution of the model was estimated to be approximately 30 Å according to the 3σ FSC criterion, being restricted partly by the relatively low size of the dataset used for the analysis and the lack of sufficient random orientations of the complex on the TEM grid. Both of these limitations reflect the use of samples prepared for TEM by negative staining and can, in principle, be overcome by using unstained vitrified samples and associated cryo-TEM techniques, as shown for the $C_2S_2$ supercomplex [18,19]. Nonetheless, this is the first time that such a large PSII–LHCII supercomplex has been shown in 3D from solubilized thylakoids in pea (*P. sativum*). The 3D reconstructions presented here once more confirm the central positioning of the $C_2S_2$ supercomplex within the larger volume of the $C_2S_2M_2$ molecular envelope and the relative positioning of various major subunits. Previous modelling of the major components of the $C_2S_2M_2$ supercomplex was presented on the final 2D projection map obtained for this supercomplex isolated from Arabidopsis by Caffarri et al. [15]. The modelling in our corresponding 3D electron density map obtained from pea is very similar to that proposed by Caffarri et al. [15], with the exception of a rotationally different position of the LHCII S-trimer, which differs by about +15° with respect to the PSII RC core. The density for the OEC proteins was not fully resolved, hence making it difficult at this stage to suggest the location of the PsbP, PsbQ and PsbR subunits, albeit these polypeptides are present within the $C_2S_2M_2$ particles analysed. An improved dataset, ideally derived from cryo-TEM, will be required to resolve and assign the OEC proteins as well as to gain fine details of the overall structure of the $C_2S_2M_2$ supercomplex.

Supplementary data to this article can be found online at http://dx.doi.org/10.1016/j.bbabio.2013.11.004.

## Acknowledgements

This work was supported by funds from the European Commission (ArtipHyction project (303435) FCH-JU-2011-1; Eco$^2$CO$_2$ project (309701) FP7-NMP2012). We thank Dr. Waidelich Dietmar (AB SCIEX-Darmstadt, Germany) for kindly performing MALDI-TOF/TOF analyses.

## References

[1] C. Pagliano, G. Saracco, J. Barber, Structural, functional and auxiliary proteins of photosystem II, Photosynth. Res. 116 (2013) 167–188.
[2] K.-H. Rhee, E.P. Morris, J. Barber, W. Kühlbrandt, Three-dimensional structure of the plant photosystem II reaction centre at 8 Å resolution, Nature 396 (1998) 283–286.
[3] B. Hankamer, E.P. Morris, J. Nield, C. Gerle, J. Barber, Three-dimensional structure of the photosystem II core dimer of higher plants determined by electron microscopy, J. Struct. Biol. 135 (2001) 262–269.
[4] K. Ifuku, T. Nakatsu, H. Kato, F. Sato, Crystal structure of the PsbP protein of photosystem II from *Nicotiana tabacum*, EMBO Rep. 5 (2004) 362–367.
[5] V. Calderone, M. Trabucco, A. Vujicić, R. Battistutta, G.M. Giacometti, F. Andreucci, R. Barbato, G. Zanotti, Crystal structure of the PsbQ protein of photosystem II from higher plants, EMBO Rep. 4 (2003) 900–905.
[6] M. Balsera, J.B. Arellano, J.L. Revuelta, J. De Las Rivas, J.A. Hermoso, The 1.49 Å resolution crystal structure of PsbQ from photosystem II of *Spinacia oleracea* reveals a PPII structure in the N-terminal region, J. Mol. Biol. 350 (2005) 1051–1060.
[7] S. Jansson, The light-harvesting chlorophyll a/b binding proteins, Biochim. Biophys. Acta 1184 (1994) 1–19.
[8] G. Jackowski, K. Kacprzak, S. Jansson, Identification of Lhcb1/Lhcb2/Lhcb3 heterotrimers of the main light-harvesting chlorophyll a/b-protein complex of photosystem II (LHCII), Biochim. Biophys. Acta 1504 (2001) 340–345.
[9] S. Caffarri, R. Croce, L. Cattivelli, R. Bassi, A look within LHCII: differential analysis of the Lhcb1-3 complexes building the major trimeric antenna complex of higher-plant photosynthesis, Biochemistry 43 (2004) 9467–9476.
[10] Z.F. Liu, H.C. Yan, K.B. Wang, T.Y. Kuang, J.P. Zhang, L.L. Gui, X.M. An, W.R. Chang, Crystal structure of spinach major light-harvesting complex at 2.72 Å resolution, Nature 428 (2004) 287–292.
[11] J. Standfuss, A.C.T. van Scheltinga, M. Lamborghini, W. Kühlbrandt, Mechanisms of photoprotection and nonphotochemical quenching in pea light harvesting complex at 2.5 Å resolution, EMBO J. 24 (2005) 918–928.
[12] X. Pan, M. Li, T. Wan, L. Wang, C. Jia, Z. Hou, X. Zhao, J. Zhang, W. Chang, Structural insights into energy regulation of light-harvesting complex CP29 from spinach, Nat. Struct. Mol. Biol. 18 (2011) 309–316.
[13] J.P. Dekker, E.J. Boekema, Supramolecular organization of thylakoid membrane proteins in green plants, Biochim. Biophys. Acta 1706 (2005) 12–39.
[14] E.J. Boekema, B. Hankamer, D. Bald, J. Kruip, J. Nield, A.F. Boonstra, J. Barber, M. Rogner, Supramolecular structure of the photosystem II complex from green plants and cyanobacteria, Proc. Natl. Acad. Sci. U. S. A. 92 (1995) 175–179.
[15] S. Caffarri, R. Kouřil, S. Kereïche, E.J. Boekema, R. Croce, Functional architecture of higher plant photosystem II supercomplexes, EMBO J. 28 (2009) 3052–3063.
[16] E.J. Boekema, H. van Roon, F. Calkoen, R. Bassi, J.P. Dekker, Multiple types of association of photosystem II and its light-harvesting antenna in partially solubilized photosystem II membranes, Biochemistry 38 (1999) 2233–2239.
[17] S. Barera, C. Pagliano, T. Pape, G. Saracco, J. Barber, Characterization of PSII–LHCII supercomplexes isolated from pea thylakoid membrane by one-step treatment with α- and β-dodecyl-D-maltoside, Phil. Trans. R. Soc. B 67 (2012) 3389–3399.
[18] J. Nield, E.V. Orlova, E.P. Morris, B. Gowen, M. van Heel, J. Barber, 3D map of the plant photosystem two supercomplex obtained by cryoelectron microscopy and single particle analysis, Nat. Struct. Biol. 7 (2000) 44–47.
[19] J. Nield, M. Balsera, J. De Las Rivas, J. Barber, Three-dimensional electron cryo-microscopy study of the extrinsic domains of the oxygen-evolving complex of spinach: assignment of the PsbO protein, J. Biol. Chem. 277 (2002) 15006–15012.
[20] J. Nield, J. Barber, Refinement of the structural model for the photosystem II supercomplex of higher plants, Biochim. Biophys. Acta 1757 (2006) 353–361.
[21] A.E. Yakushevska, P.E. Jensen, W. Keegstra, H. van Roon, H.V. Scheller, E.J. Boekema, J.P. Dekker, Supermolecular organization of photosystem II and its associated light-harvesting antenna in *Arabidopsis thaliana*, Eur. J. Biochem. 268 (2001) 6020–6028.
[22] C. Pagliano, S. Barera, F. Chimirri, G. Saracco, J. Barber, Comparison of the α and β isomeric forms of the detergent n-dodecyl-D-maltoside for solubilizing photosynthetic complexes from pea thylakoid membranes, Biochim. Biophys. Acta 1817 (2012) 1506–1515.
[23] D.J. Arnon, Copper enzymes in isolated chloroplasts, polyphenoloxidase in *Beta vulgaris*, Plant Physiol. 24 (1949) 1–14.
[24] H. Schagger, G. von Jagow, Blue native electrophoresis for isolation of membrane protein complexes in enzymatically active form, Anal. Biochem. 199 (1991) 223–231.
[25] U.K. Laemmli, Cleavage of structural proteins during the assembly of the head of bacteriophage T4, Nature 227 (1970) 680–685.
[26] Y. Kashino, H. Koike, K. Satoh, An improved sodium dodecyl sulfate-polyacrylamide gel electrophoresis system for the analysis of membrane protein complexes, Electrophoresis 22 (2001) 1004–1007.
[27] U. Hellmann, C. Wernstedt, J. Gonez, C.H. Heldin, Improvement of an "In-Gel" digestion procedure for the micropreparation of internal protein fragments for amino acid sequencing, Anal. Biochem. 224 (1995) 451–455.
[28] C. Pagliano, F. Chimirri, G. Saracco, F. Marsano, J. Barber, One-step isolation and biochemical characterization of a highly active plant PSII monomeric core, Photosynth. Res. 108 (2011) 33–46.
[29] A. Shevchenko, S. Sunyaev, A. Loboda, A. Shevchenko, P. Bork, W. Ens, K.G. Standing, Charting the proteomes of organisms with unsequenced genomes by MALDI-quadrupole time-of flight mass spectrometry and BLAST homology searching, Anal. Chem. 73 (2001) 1917–1926.
[30] G. Tang, L. Peng, P.R. Baldwin, D.S. Mann, W. Jiang, I. Rees, S.J. Ludtke, EMAN2: an extensible image processing suite for electron microscopy, J. Struct. Biol. 157 (2007) 38–46.
[31] M. van Heel, G. Harauz, E. Orlova, R. Schmidt, M. Schatz, A new generation of the IMAGIC image processing system, J. Struct. Biol. 116 (1996) 17–24.
[32] P. Dube, P. Tavares, R. Lurz, M. van Heel, The portal protein of bacteriophage SPP1: a DNA pump with 13-fold symmetry, EMBO J. 12 (1993) 1303–1309.
[33] M. Van Heel, Angular reconstitution: a posteriori assignment of projection directions for 3D reconstruction, Ultramicroscopy 21 (1987) 111–123.
[34] M. Radermacher, Three-dimensional reconstruction of single particles from random and nonrandom tilt series, J. Electron. Microsc. Tech. 9 (1988) 359–394.
[35] M. van Heel, M. Schatz, Fourier shell correlation threshold criteria, J. Struct. Biol. 151 (2005) 250–262.
[36] E.F. Pettersen, T.D. Goddard, C.C. Huang, G.S. Couch, D.M. Greenblatt, E.C. Meng, T.E. Ferrin, UCSF chimera—a visualization system for exploratory research and analysis, J. Comput. Chem. 25 (2004) 1605–1612.
[37] K.N. Ferreira, T.M. Iverson, K. Maghlaoui, J. Barber, S. Iwata, Architecture of the photosynthetic oxygen-evolving center, Science 303 (2004) 1831–1838.
[38] J. De Las Rivas, J. Barber, Analysis of the structure of the PsbO protein and its implications, Photosynth. Res. 81 (2004) 329–343.
[39] Y. Umena, K. Kawakami, J.R. Shen, N. Kamiya, Crystal structure of oxygen-evolving photosystem II at a resolution of 1.9 Å, Nature 473 (2011) 55–60.
[40] T.M. Bricker, W.R. Odom, C.B. Queirolo, Close association of the 33-kDa extrinsic protein with the apoprotein of Cpa1 in photosystem II, FEBS Lett. 231 (1988) 111–117.
[41] I. Enami, T. Miyaoka, Y. Mochizuki, J.R. Shen, K. Satoh, S. Katoh, Nearest neighbor relationships among constituent proteins of oxygen-evolving photosystem II membranes — binding and function of the extrinsic 33 kDa protein, Biochim. Biophys. Acta 973 (1989) 35–40.
[42] A. Seidler, A.W. Rutherford, H. Michel, On the role of the N-terminus of the extrinsic 33 kDa protein of photosystem II, Plant Mol. Biol. 31 (1996) 183–188.

[43] K. Ifuku, K. Ido, F. Sato, Molecular functions of PsbP and PsbQ proteins in the photosystem II supercomplex, J. Photochem. Photobiol. B 104 (2011) 158–164.
[44] Y. Allahverdiyeva, M. Suorsa, F. Rossi, A. Pavesi, M.M. Kater, A. Antonacci, L. Tadini, M. Pribil, A. Schneider, G. Wanner, D. Leister, E.M. Aro, R. Barbato, P. Pesaresi, Arabidopsis plants lacking PsbQ and PsbR subunits of the oxygen-evolving complex show altered PSII super-complex organization and short-term adaptive mechanisms, Plant J. 75 (2013) 671–684.
[45] X.P. Li, O. Björkman, C. Shih, A.R. Grossman, M. Rosenquist, S. Jansson, K.K. Niyogi, A pigment-binding protein essential for regulation of photosynthetic light harvesting, Nature 403 (2000) 391–395.
[46] S. Kereïche, A.Z. Kiss, R. Kouřil, E.J. Boekema, P. Horton, The PsbS protein controls the macro-organisation of photosystem II complexes in the grana membranes of higher plant chloroplasts, FEBS Lett. 584 (2010) 759–764.
[47] J. Nield, C. Funk, J. Barber, Supermolecular structure of photosystem II and location of the PsbS protein, Phil. Trans. R. Soc. B 355 (2000) 1337–1344.
[48] J. Sharma, M. Panico, J. Barber, H.R. Morris, Characterization of the low molecular weight photosystem II reaction center subunits and their light-induced modifications by mass spectrometry, J. Biol. Chem. 272 (1997) 3935–3943.
[49] D. Zheleva, J. Sharma, M. Panico, H.R. Morris, J. Barber, Isolation and characterization of monomeric and dimeric CP47-reaction center photosystem II complexes, J. Biol. Chem. 273 (1998) 16122–16127.
[50] M. Plöscher, B. Granvogl, M. Zoryan, V. Reisinger, L.A. Eichacker, Mass spectrometric characterization of membrane integral low molecular weight proteins from photosystem II in barley etioplasts, Proteomics 9 (2009) 625–635.
[51] P. Dainese, R. Bassi, A supramolecular light-harvesting complex from chloroplast photosystem-II membranes, Eur. J. Biochem. 204 (1992) 317–326.
[52] N. Betterle, M. Ballottari, S. Zorzan, S. de Bianchi, S. Cazzaniga, L. Dall'osto, T. Morosinotto, R. Bassi, Light-induced dissociation of an antenna hetero-oligomer is needed for non-photochemical quenching induction, J. Biol. Chem. 284 (2009) 15255–15266.